THE INTERNATIONAL JOURNAL OF MEDICAL ROBOTICS AND COMPUTER ASSISTED SURGERY
Int J Med Robotics Comput Assist Surg 2010; **6**: 444–453.
Published online 2 September 2010 in Wiley Online Library (wileyonlinelibrary.com) **DOI:** 10.1002/rcs.354

ORIGINAL ARTICLE

Introducing haptic capabilities to a bone-mounted robot for intra-operative surface scanning

Yoel Shapiro*
Alon Wolf

BRML Biorobotics and Biomechanics Laboratory, Department of Mechanical Engineering, Technion–Israel Institute of Technology, Haifa, Israel 32000

*Correspondence to: Yoel Shapiro, BRML Biorobotics and Biomechanics Laboratory, Department of Mechanical Engineering, Technion–Israel Institute of Technology, Haifa, Israel 32000.
E-mail: yoelsh@tx.technion.ac.il

Accepted: 1 August 2010

Abstract

Background Bone-mounted robots for orthopaedic surgery are small, cost-effective and could reduce invasiveness. Preoperative planning requires imaging (e.g. X-ray, CT, MRI) and a registration procedure, which introduces error. Accuracy might be improved by building an intraoperative anatomical model in the robot's own coordinate system, utilizing the rigid bone–robot connection.

Methods Haptic capabilities were added to MBARS and user tests were conducted to help design the haptic control loop. The accuracy of a 3D physical scan was tested on a femur model.

Results Indication for force scaling and mode switching was found. Average distance error of collected points from the surface scanned by the robot was 0.3 mm.

Conclusions It is suggested that haptic control of bone-mounted robots should be non-linear and not necessarily transparent. Haptic surface acquisition can be used to generate an accurate intraoperative model of a joint surface. Copyright © 2010 John Wiley & Sons, Ltd.

Keywords medical robotics; orthopaedic surgery; haptic control; knee arthroplasty; surface reconstruction

Introduction

Surgical robotics is a promising avenue to improve medical treatment and is expected to play a major role in the operating room of the future (1). In 1992, orthopaedic surgery was one of the first medical fields to adopt surgical robotics (2), the pioneer system being Robodoc (3). Most orthopaedic procedures are arthritis-related, including knee and hip replacement (arthroplasty). Arthritis is a major age-related health concern, imposing a significant economic burden on Western countries (4). Several robotic systems have been developed to improve the accuracy of bone resurfacing and implant alignment during knee replacement (5) and to make the procedure less invasive (6). Early medical robots resembled stand-alone industrial robots and required a registration procedure in order to correlate information from preoperative medical imaging to the robot and patient. Wolf *et al*. (7) were among the first to introduce the concept of a bone-mounted robot for spinal operations. This study later resulted in the FDA-approved SpineAssist robot (8). Other orthopaedic surgical systems followed this concept, such as Praxiteles (9) and MBARS (10) (two bone-mounted robots for knee joint arthroplasty). Advantages of bone-mounted

robots include dramatically reduced size of the robotic system and reduced cost. In addition, the base of a bone-mounted system is attached in rigid manner to the operation site, so errors induced by dynamic tracking can be avoided. The bone-mounted concept could present even more advantages. This research developed a method allowing a bone-mounted system to explore the surgical target without relying on pre-operative medical imaging. MBARS was used as a study case, continuing the work previously published here (10). A teleoperated haptic interface was designed for intuitive manual control. The new system enables digitizing and describing the joint surface in the robot's own coordinate space. The MBARS set-up is shown in Figure 1.

Designing a surface-scanning algorithm for a general, unknown object, 'probing in the dark', would probably be time-consuming and ineffective. However, converting to a telerobotic or semi-active system allows harnessing human intelligence and the surgeon's expertise to this task. In a telerobotic system the operator can use his experience to directly move a *master* mechanism, which is followed by the *slave* mechanism, and focus on the region of interest and its distinctive features. In this study a bone-mounted robot was adjusted to work as a telerobotic system with haptic feedback. User tests were employed to adjust the system's control according to users' feedback, under the constraints implied by the robot being bone-attached. The final design of the control loop is surprisingly different than expected from an ideal haptic apparatus. A bone scanning example is presented to demonstrate feasibility of intraoperative joint-surface mapping.

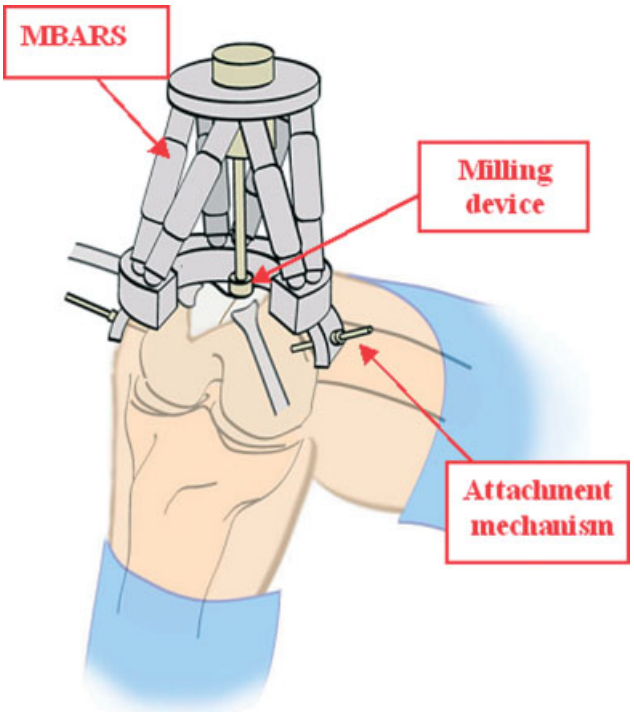

Figure 1. MBARS mounted on femur

Background

In a telerobotic system two mechanisms provide an interface between the scanned object and the surgeon, who cannot feel the object directly or, in this case, sense the interaction between the medical instrument and the knee joint surface. This sensory deprivation may be compensated for by various feedback modalities [see examples in (11–13)], including haptic feedback. 'Haptic' is a Greek word referring to the sense of touch; in the present case, we want to use forces to convey geometric constraints induced by the joint surface, as shown in Figure 2, back to the human operator.

Haptics has been shown to contribute to the efficiency and safety of medical robotic systems (11) and seems to be preferred over other modalities, at least by non-expert users (14). Advantages include shorter neural processing time and the fact that haptics does not demand attention from the same senses already burdened by the myriad signals in a typical operating theatre, i.e. the profusion of beeps and flashes emitted by other medical instruments and monitors.

Yokokohji and Yoshikawa (15) defined widely used indices for haptic systems which, when equal to zero, assure that the master and slave follow the same trajectory (J_p) or that the master reflects interaction forces from the slave side accurately (J_f). Using an ideal haptic system, the user would feel as though he/she was operating on the target directly and the mechanisms in between would be transparent – indeed, haptic performance is often referred to as 'transparency'. Hogan (16) explored the basics for stable robotic manipulation and defined a general approach termed 'impedance control' – shaping a trade-off between position accuracy and actuation force. Similarly, another common transparency goal is to reflect identical impedance on the master side to that encountered by the slave when interacting with the environment.

The most general haptic architecture is the four-channel architecture (17), where a double hybrid signal, including force and motion, is sent from master to slave and vice versa, but many haptic systems make use of fewer channels, usually two. Stability and performance are contradicting goals, so the additional freedom provided by using four channels instead of two could be used to improve this trade-off. Of course, reducing time delays and quantization errors would improve both

Figure 2. A general haptic system

DOI: 10.1002/rcs

stability and performance, often at a much higher cost. Theoretical study of haptic systems usually assumes that the user and environment can be considered as passive elements with a bounded response (17) and then tries to ensure that the master–slave dyad be perfectly stable with maximal transparency. This somewhat conservative approach usually recommends introducing damping as a means to ensure stability. A specific damping ratio might be determined based on a system's transfer function (18–20), wave variable analysis and passivity considerations (21). Even varying damping can be introduced by a passivity controller (22). In practice, the user is far from passive and can play a vital role in stabilizing the master side by instinctively changing arm stiffness and damping ratio [for more on the human arm, see (23–25)]. A clear and comprehensive analysis of stability and performance of haptic systems is given in (26) for various combinations of manipulators from different types, working under four- or two-channel architecture. Because manipulation has a dual nature, going from free motion to constrained motion when impacting an object, some researchers resorted to non-linear solutions. Haptic telerobotic drilling systems often realize non-linear control solutions; see mode switching in (27) or adaptive gains in (28). In this research, gain scheduling was adopted by switching between a pair of two-channel architectures on transition from free to constrained motion, and the other way round. The constraints and considerations for designing a haptic feedback loop for a bone-attached robot are explained in Materials and methods.

Materials and Methods

The system's main components are the master, the slave and a six degree-of-freedom (DoF) force and torque (FT) sensor mounted along the slave's probe, all shown in Figure 3. The laboratory system is not yet operation room (OR)-compatible.

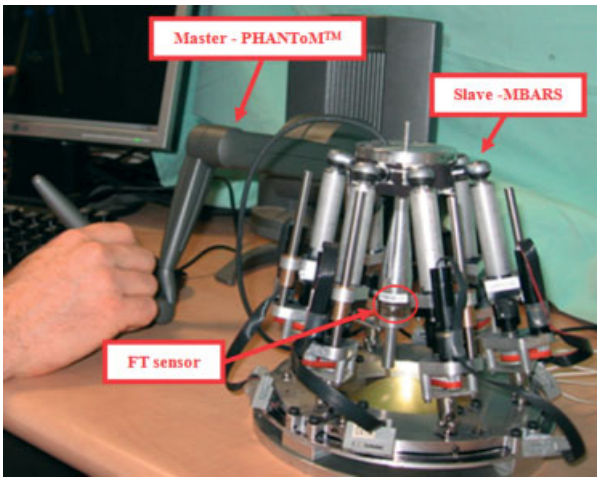

Figure 3. System main components

All communications are handled via a PC which serves as the controller, working with a real-time UNIX operating system. Communication with the actuators (I^2C, six PIC microcontrollers) imposes a 40 Hz bottleneck; all other communications and computations run at ~100 Hz. It should be kept in mind that 40 Hz is still above voluntary hand motion frequencies [<12 Hz (29)].

The two most important features that allow mounting the slave on the anatomy are its miniature size and light weight, e.g. MBARS weighs ~1 kg, its base is 15 cm in diameter and its initial height is ~16 cm. The small size induces constraints on the mechanical design of the robot mechanism. More specifically, a high gear ratio in necessary to withstand deburring forces when using small motors. MBARS actuators are easily position controlled, while force control is impractical, mainly due to friction. When Hogan applied impedance control (30) he used direct-drive actuators, but these would be too big for a bone-mounted robot. Adding a FT sensor [ATI, Nano 17, non-sterile (31)] along the slave's probe bypassed the actuators and simplified obtaining contact forces. FT readings were treated for noise by filtering and applying an amplitude threshold. The torques were discarded as the master can only reflect forces.

A commercially available haptic interface was chosen to serve as the master – PHANToM™, Desktop. PHANToM is generic and widely used for haptic research and medical simulators, including drilling simulation, as in (32,33). The master has very low inertia and is highly back-drivable, meaning that force applied by the human user should immediately be manifested in the master's position. However, this master lacks a simple, accurate method to assess the forces applied by the human user (e.g. force sensor, verified dynamic model) so, as in most medical haptic systems, the command to the slave consisted of a position signal only.

The slave's high gear ratio presents a tight speed limit (~20 mm/s in the x and y and ~5 mm/s in the z direction) so position signals were considered and not velocity signals. The controller implemented mode-switching between a couple of two-channel architectures. Adhering to the terminology presented in (26), our system can be classified as having a two-channel, impedance-admittance architecture, operating in a position–position (PP) mode while in free motion, and switching to a position–force (PF) mode under constrained motion, i.e. the command from master to slave consists only of a position command, while the feedback from slave to master–user end might include position and/or force, as shown in Figure 4, where *Fe* stands for the environment's

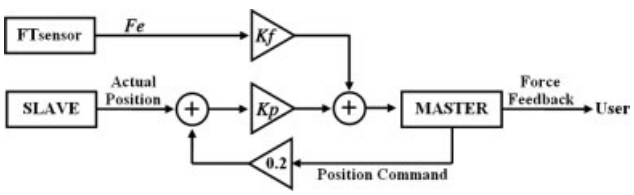

Figure 4. Feedback from slave to master–user end

DOI: 10.1002/rcs

reaction force, *Kf* and *Kp* are the gain factors of *Fe* and position error (*PE*), respectively. *PE* is calculated by subtracting the position command from the real-time solution of the slave's inverse kinematics. This means that the *PE* signal points towards the slave's actual position, pulling the user back when the slave lags behind, thus demonstrating to the user that he/she should slow down. In free motion *PE* was used, since any force reading would be merely noise, but during contact only *Fe* was reflected, since *PE* 'distorts' the surface being probed. Some results supporting this choice are presented later in the Discussion.

The bone-mounted slave is naturally more stable and did not require special attention. Practical difficulties prevented theoretical analysis of our system – lack of a dynamic model of the master and MBARS velocity saturation, which is anisotropic. Instead users' comments were relied upon for determining appropriate gains, and when comparing different control architectures some empirical indices were considered as well (see instability index in Results and Figure 13 in the Discussion; not shown here are tracking accuracy and completion time).

The master's workspace is significantly larger than the slave's and it can move much faster, so the position command was scaled down by a factor of five. The scaling impairs transparency but, since the user has a direct view of the target, it seems to be very convenient. In fact, the scaling down serves as a magnifying glass and actually improves the accuracy achieved. Because of the motion reduction, tracking accuracy was estimated as the discrepancy between the downscaled position command and the slave's actual position. The slave's communication protocol introduces the lowest limit on data flow, 40 Hz, which suggests a 20 Hz Nyquist frequency limit on data analysis. Since human motion is usually bound by 12 Hz (29), the 40 Hz limit does not interfere with motion. The master and FT sensor communicate at above 100 Hz, which compares to the higher levels of human sensatory frequencies [except for texture; see more on texture display in (34,35)]. Instability phenomena observed in this research included slow (~1 Hz) bouncing of the slave under constant contact or sudden hand jerks (10–50 mm long) which sometimes occurred upon MBARS impacting a surface. Notice that because of the slave's mechanical response time, high frequency disturbances on the master side (jerks) manifested as motions of a much lower frequency on the slave's side. To withstand deburring forces, the bone-mounted slave is highly geared and position controlled; this design results in high interaction forces when probing a surface (magnitude up to 10 N). While MBARS can control its position accurately while withstanding such impacts, a human user would find it difficult. In order to 'scale down' the interaction forces, a unidirectional compliant tip was designed for the slave's probe, shown in Figure 5. Unlike the artificial motion scaling, the tip's compliance physically reduces the interaction forces. The compliance must be compensated for when registering points on the constraining surface, by considering the force component parallel to the probe and the spring's coefficient. The force sensor is mounted along the probe, right above the compliant tip, so the total probe length includes its base, the sensor, and the compliant tip.

Smooth mode switching was implemented via smooth scheduling gains (SG; C_{Fe}, C_{PE}), as shown in Figure 6. The reaction force amplitude was used as a scheduling variable, able to detect contact and distinguish between free and constrained motion.

A general formula for the SG was used, as expressed in equation (1), where no relation between the two SGs is presumed:

$$C_{Fe} = 0.5\left[1 + \tanh\left(S_{Fe}\left(\|Fe\| - Th_{Fe}\right)\right)\right]$$
$$C_{PE} = 0.5\left[1 + \tanh\left(S_{PE}\left(Th_{PE} - \|Fe\|\right)\right)\right] \quad (1)$$

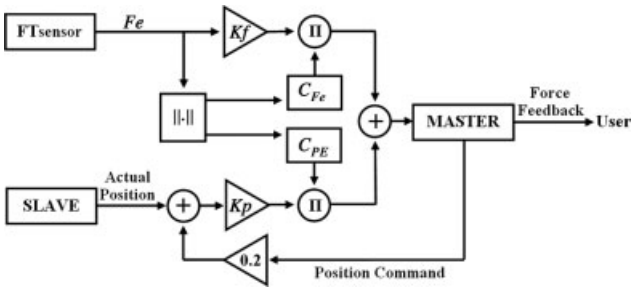

Figure 6. Feedback from slave to master–user end, with gain scheduling

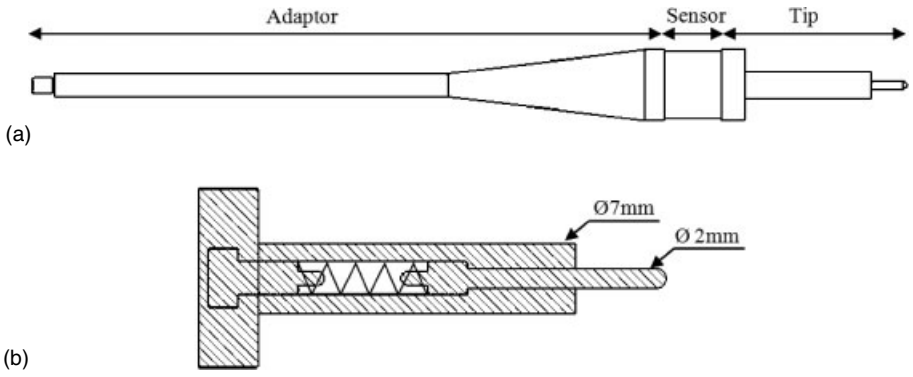

Figure 5. (a) Whole probe; (b) section view of unidirectional compliant tip

DOI: 10.1002/rcs

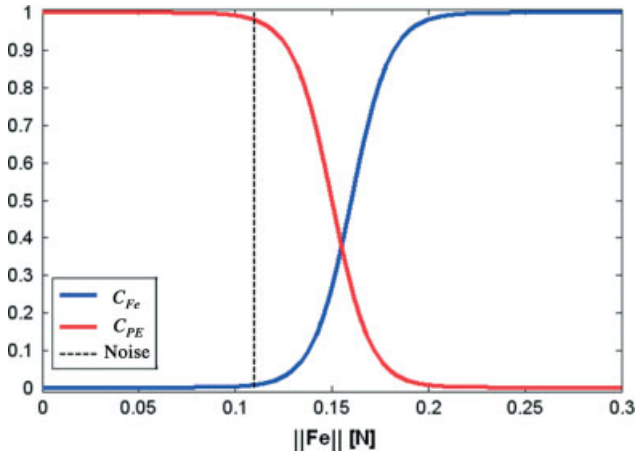

Figure 7. Scheduling gains for $Th_{Fe} = 0.16[N]$, $S_{Fe} = 50[1/N]$, $Th_{PE} = 0.15[N]$, $S_{PE} = 50[1/N]$

where *Fe* represents the reaction forces (treated reading from the FT sensor), Th_{Fe} and Th_{PE} are scheduling thresholds and are a symmetry point of each scheduling variable, S_{Fe} and S_{PE} are the slopes at the scheduling threshold and give an indication of how fast the switching is, i.e. almost full switching, takes place within a $1/S_{Fe}$ N range. The switching parameters were determined to assure 'pure' force feedback already at a low level of 0.2 N and to avoid the 0.11 N noise threshold, as shown in Figure 7.

User tests aimed at fine-tuning the system employed a 3D model, shown in Figure 8. In order to display a path to the user without affecting the model's surface, a transparent material was chosen for the surface and a subterranean cavity was filled with a colourful substance. Volunteers included nine males and two females, 10 right-handed and one left-handed (male), aged 21–39, all with very little or no haptic experience. The slave was limited to three DoF, i.e. worked at a set orientation.

Experiments

First experiment type: full contact

To give the volunteers the feel of the haptic system, they were asked to follow the path three times, as fast as possible, without exceeding its boundaries and while maintaining contact. This was done at five different *Kp* (position-error gain) values, while *Kf* (force gain) was set to zero, reflecting to the user-only position errors. A short break was given between each trial. The procedure was repeated, this time at five values of *Kf* while *Kp* was set to zero, reflecting to the user-only reaction forces.

Second experiment type: personal tuning

Next, the volunteers were asked to determine their preferred gain values. They were allowed to move the slave in the air while *Kp* was increased and decreased several times (0.00–0.30 N/mm range, 0.05 N/mm increments), until the volunteer was satisfied. *Kf* was determined similarly (0.0–1.0 range, 0.1 increments) when the slave was moved while maintaining contact with the test surface. Under gain scheduling, either force feedback or position feedback is reflected to the user while the other modality is blocked, except for transitional phases which are dominated by the four gain scheduling parameters (Th_{Fe}, Th_{PE}, S_{Fe}, S_{PE}). Therefore each gain was determined independently, i.e. while the complementary gain was set to zero.

Third experiment type: tapping

Finally the volunteers were asked to follow the rectangular path three times as fast as possible without touching the surface except for a quick tap at each corner. The tapping task examined what happens in transition from free to constrained motion and vice versa. The evaluation criterion was an empirical instability index – see Appendix for a detailed description. Each volunteer performed three repetitions of this task under slightly different conditions – without gain scheduling (i.e. with constant gains; see Figure 4), with gain scheduling (see Figure 6) and with gain scheduling and non-linear damping. The damping was non-linear in the sense that it was applied to the feedback force only when a direction change was noticed, i.e. the feedback at a given point in time pointed in the opposite side of the plane defined by the feedback in the previous moment and lasted only 0.5 s. This condition was met when detaching from a surface, showing a 'quicksand' or 'sticky' effect. It was suspected

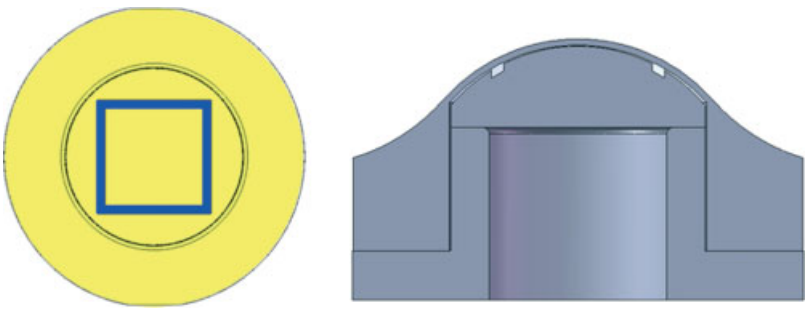

Figure 8. Top view (colour) and mid-section (greyscale) of test surface

DOI: 10.1002/rcs

that these sudden direction changes seemed to surprise the user (as opposed to changes in amplitude), preventing stabilization via instinctive arm-impedance adaptation.

Fourth experiment type: surface acquisition

Besides user tests, initial testing of surface acquisition was performed on a femur model. The scanned points were compared to a laser scan of the joint surface. The best fit between the points from the haptic scan and the laser scan was computed, using the improved iterative closest point (ICP) algorithm presented in (36). The ICP version in (36) takes into consideration not only the distances between the cloud of points and the surface but also the orientations of the surface-normals of a matched pair of points. The cost function is given in equation (2):

$$F(R,t) = \frac{1}{N}\sum_{i=1}^{N} \alpha_i \left\| M_i - (RD_i + t) \right\|^2 + \frac{1}{N}\sum_{i=1}^{N} \beta_i \left\| n_{M_i} - Rn_{D_i} \right\|^2 \quad (2)$$

where F is the cost function, R is a 3×3 rotation matrix, t a 3×1 translation vector, D_i is a data point and M_i is its closest neighbour on the model, n_{Di} and n_{Mi} are surface-normal to these points, respectively, and α and β are weighting factors. Estimating n_{Di} – the surface-normals at the collected data points – is done by normalizing the interaction force. To eliminate friction effects, the projection of the normal on the slave's instantaneous velocity was subtracted and then it was renormalized, thus correcting the surface-normals according to equation 3:

$$\tilde{n}_{Di} = \frac{n_{Di} - (n_{Di} \cdot v_i)v_i}{\left\| n_{Di} - (n_{Di} \cdot v_i)v_i \right\|} \quad (3)$$

where $\sim$ marks the corrected normal, n_{Di} is the original normal obtained from the reaction force and v_i is the local velocity.

Results

As expected from the first experiment, users found it difficult to maintain contact when following a path along a surface with only *PE* feedback, in comparison to only force feedback. The contact time percentage of eight different users is compared in Figure 9 under force or *PE* feedback at different gains. The results of each volunteer, at each gain value, are shown with a different marker, and the dotted line shows the median of all users (at that gain). Most users maintained 100% contact under force control, so their markers hide each other.

The gains picked by different volunteers in the second experiment are shown in Figure 10 as an x–y scatter. Two gain pairs were chosen by more than one volunteer; this information is shown immediately above these two points ((0.05, 0.7), (0.1, 0.8)) in Figure 10; the mean gain values are depicted by a red asterisk to help assess their increased weight. The mean gain values are $Kf = 0.70 \pm 0.15$, $Kp = 0.11 \pm 0.05$. Notice that under all gain-pairs chosen, interaction forces are reduced ($Kf < 1$) and that the virtual spring represented by Kp is quite weak; ~0.1 N/mm after scaling down, equivalent to 0.02 N/mm on the master side.

In the tapping experiment (third experiment type), volunteers were asked to approach the surface going down along the z axis. The instability indices were examined for each direction: $IS_{x\backslash y\backslash z}$, x goes from left to right, y from forward to backward and z is up-down (see Appendix for more on *IS*). The scheduling regime had a mixed effect on IS_z but IS_x and IS_y were hardly affected by changes, yet remained quite typical *for each user*. The personal patterns might suggest that control parameters should be tailored per user. For example, should anisotropic position-error gain be used to stabilize each user's weaker direction? In the Discussion, we suggest a generic solution instead. A scatter plot of $IS_x - IS_y$ is shown in Figure 11. Each marker type in Figure 11 depicts the three trials of the same volunteer.

Perhaps the most interesting result is the fit between points physically scanned by the slave and joint surface,

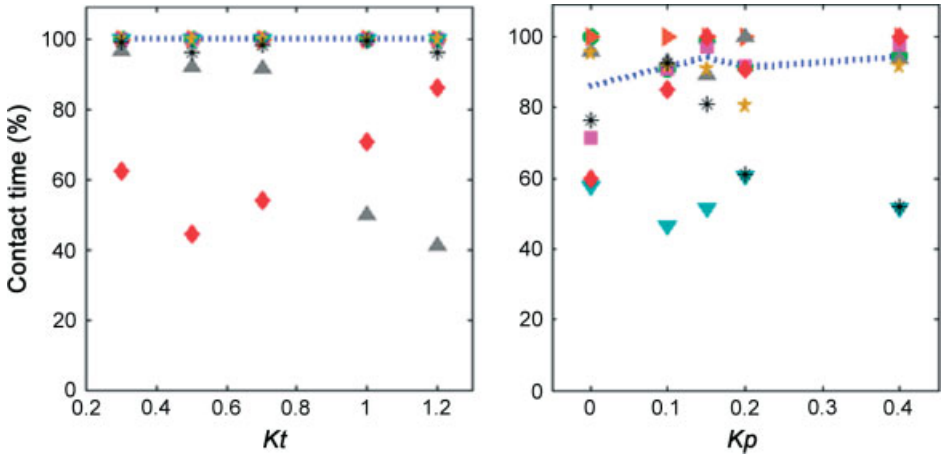

Figure 9. Percentage of contact time under force feedback (left) and PE feedback (right)

DOI: 10.1002/rcs

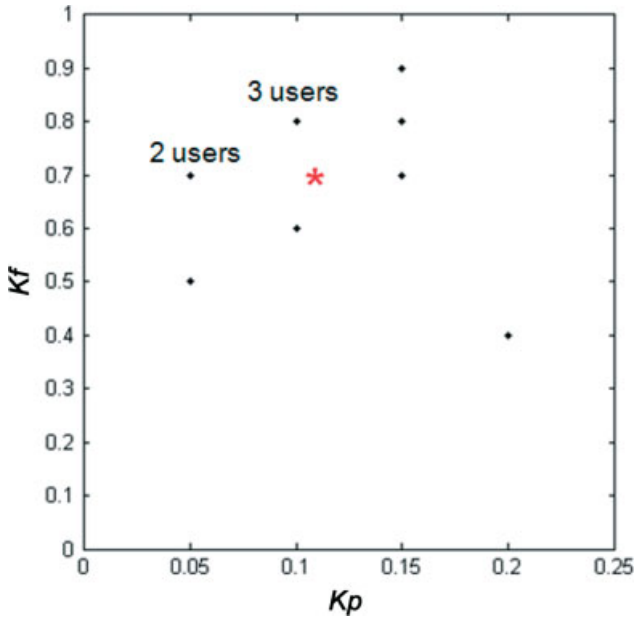

Figure 10. Gain-coefficient pairs

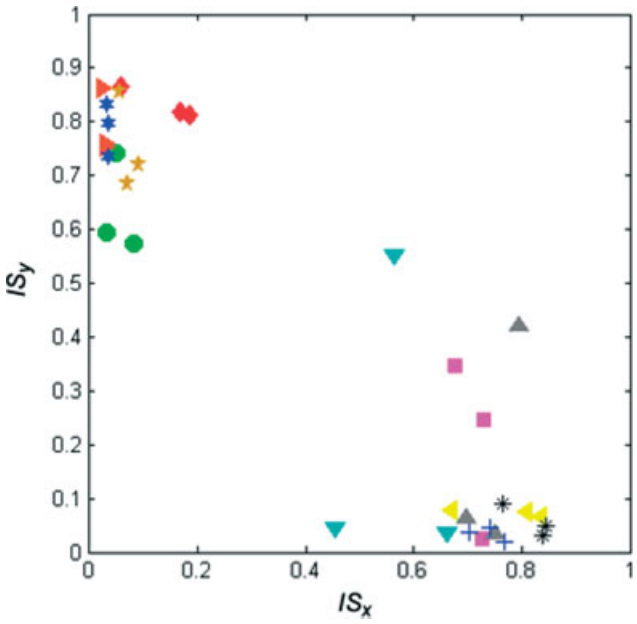

Figure 11. Instability in *x*–*y* directions of each volunteer's tapping experiments

reconstructed from the laser scan. The fourth experiment was only conducted once, to demonstrate concept feasibility. Implementing the ICP algorithm on ~450 sampled points resulted in an average distance to surface of 0.3 mm with 1 mm STD and a maximum error of 4 mm. Notice that the tip's 2 mm diameter (Figure 5) implies ~1 mm resolution across the scanned surface. The points shown in Figure 8 were collected manually, a process that took only 1–2 min. The fit between the scanned points and the probed surface is depicted in Figure 12. The physical scan appears as green dots and normal-vectors [n_{D_i} and not $\tilde{n}_{D_i}$ – see (3)], while the joint

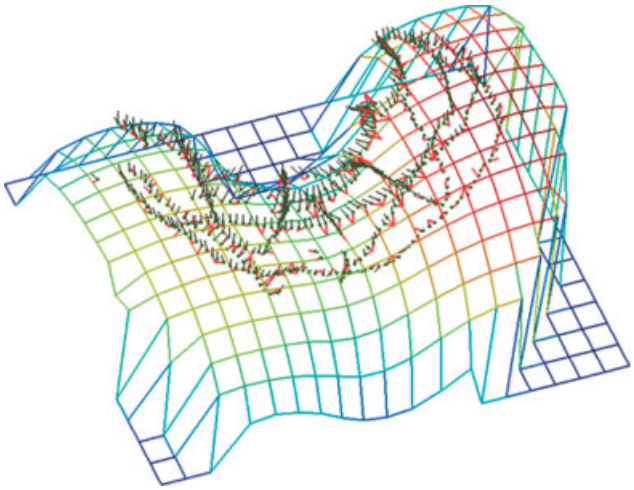

Figure 12. Fit of physical scan to bone surface

surface is displayed as a grid. The red lines show the point-to-surface distances used in the ICP cost function.

Discussion

The new CNC-like technology represented by MBARS should aid using the next generation of anatomically shaped implants. Perhaps the most exciting prospect of this research is the future potential to reconstruct, or digitize, a patient's knee joint surface intra-operatively in the OR. Collecting enough points at an adequate accuracy should provide a reliable surface reconstruction. Such an image-free technique can eliminate the need for registration of the patient's anatomy and exposure to radiation during preoperative planning, and avoid the typical tracking errors. Some procedures might benefit from improved accuracy but still require preoperative planning; e.g. considering the effect of total knee replacement (TKR) on the biomechanical axis (hip–knee–ankle). The results presented in Figure 8 are already promising, and it is believed that the errors were caused mainly by repeatability limits of MBARS' prototype version; ~0.1 mm along the tip (after compliance compensation), ~1.5 mm tangent to the tip, and under a *lateral* force exceeding 0.4 N, the probe bends at ~1.5 mm/N (currently uncompensated for). The accuracy of a reconstructed surface depends also on the local relation between surface curvature and scan density. We intended to explore in the future semi-autonomous scanning, ways to optimize the scanning time and suitable surface reconstruction techniques.

Reduced sensitivity to surfaces under PE feedback was identified (Figure 9), as expected. The measured reaction forces also indicated that users pressed against the surface much harder under PE feedback than under force feedback. The decision to introduce gain scheduling, i.e. to switch off the PE feedback during contact, is supported by the fact that PE introduces an artificial friction sensation sometimes out-shading the reaction forces, as portrayed in Figure 13; the blue line is the master's position command,

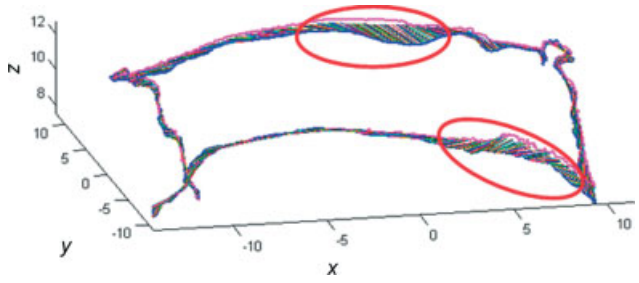

Figure 13. Portrayal of increased virtual friction without gain scheduling

the pink line is the slave's actual trajectory and the straight lines in between represent feedback to the user when no gain scheduling is present, i.e. a linear combination of PE and force feedback is reflected to the user at all times. The red ellipses draw attention to situations in which this fake friction effect is vivid.

How do the gains chosen by the volunteers correspond to common haptic goals? It would be expected that the volunteers would instinctively perform a trade-off between transparency and stability. According to (26), for the type of master–slave chosen (Impedance-Admittance), the PP architecture in free motion and PF architecture under constrained motion should be 'quite robust', so we might presume that users would emphasize transparency.

The mean value for Kp was 0.10 N/mm, which translates to 0.02 N/mm because of the motion scaling. This choice implies that the user feels a resisting force even under inherently stable free motion, which violates the common notion that the forces felt by the slave should be accurately reflected to the user. This might represent a trade-off with another performance factor suggested in (15) – that the master and slave trajectories must be similar or, in their terms, a trade-off between minimal J_p (accurate position tracking) and minimal J_f (accurate force reflection).

The average Kf value was 0.7 – less than the ideal force reflection factor of 1. The forces are not perfectly reflected and neither is the compliance of the probed surface. When contacting a hard object at a straight angle, the slave would 'feel' impedance equal to the compliant tip's spring coefficient, which is ~0.8 N/mm. However the impedance felt by the human user Kh, would be affected by the force gain Kf, the spring constant Ks and the scaling factor Sf, as in equation 4:

$$Kh = \frac{Kf}{Sf}Ks \approx \frac{0.7}{5}0.8 = 0.11\left[\frac{N}{mm}\right] \quad (4)$$

The impedance at contact is approximately five times higher than in free motion; such a difference would be easily noticeable compared to the 7% force just-noticeable-difference (JND) reported in (37).

In fact, instability was noticed mainly in transition from free motion to full contact. A smaller degree of instability was noticed when maintaining contact with an obstacle and when detaching from an object back into free motion. Users can learn to foresee the feedback jump and compensate by slowing down or stiffening their arms, but we hope to find a robust method to improve this aspect. Closer examination of the instability indices indicates that users were surprised by lateral forces; coming down towards the surface along the z axis, the jerks were mainly in the x–y plane. These lateral forces develop because the slave approaches the surface at an angle, which is a realistic scenario. We suggest that anisotropic PE feedback might be able to compensate if it were used to create a virtual fixture around the instantaneous velocity, given adequate band width.

Conclusions

The basis for a practical intraoperative method for joint surface reconstruction was presented. A hybrid gain-switching approach was used to reflect haptic feedback to the users and its advantages were demonstrated. Users picked gain factors which ensure non-zero feedback in free motion and a large JND between the perceived impedance under free motion and constrained motion. Lateral forces during transition to full contact still present a challenge.

Acknowledgements

This work was supported by the Gutwirth Fund for the Promotion of Research, Israel.

Supporting Information on the Internet

A short movie may be found in the online version of this article:

Movie. Haptic bone scan, demonstrating haptic scanning of a bone model and fitting the collected points with the ICP algorithm to a laser scan of the same model.

Appendix

Determining the stability of a trajectory from its Fourier transform is similar to the approach presented in (38), where periodograms were considered. The Fourier transform of a signal can be viewed as a time average of the periodograms. According to the Wiener–Khinchin theorem, integrating within a frequency band over the Fourier transform of a signal's auto-correlation function gives the signal's spectral power within that frequency band. The Fourier transform of the auto-correlation function is equivalent to the square of the original signal's transform amplitude. Looking for a scalar expression that is sensitive to how 'squiggly' a trajectory is led us, by trial and error, to the following normalized index:

$$IS = \frac{f_{90}}{f_{Nyquist}} \quad (5)$$

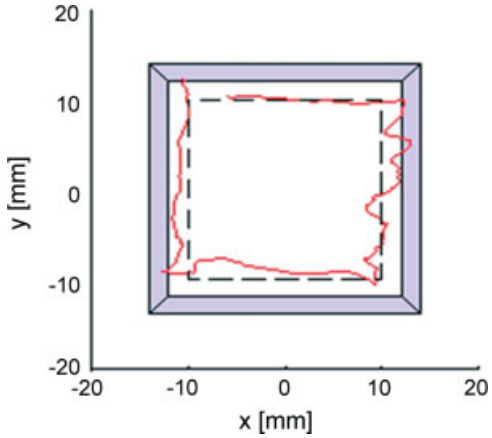

Figure 14. Example of a squiggly trajectory

where $f_{Nyquist}$ is the limit for spectral analysis capability and is equal to 20 Hz according to the slave's communication restriction and f_{90} is a percentile determined by:

$$\int_0^{f_{90}} \left| \Im\left(\overrightarrow{traj} \cdot \hat{\alpha}\right)(f) \right| df = 0.90 \cdot \int_0^{f_{Nyquist}} \left| \Im\left(\overrightarrow{traj} \cdot \hat{\alpha}\right)(f) \right| df \qquad (6)$$

where $\Im$ is used for the Fourier transform or the discrete Fourier transform for discrete signals. The instability index was calculated separately for each Cartesian component of the trajectory, hence the projection on $\hat{\alpha}$ for $\hat{\alpha} = \hat{x}, \hat{y}, \hat{z}$, where the superscript $\hat{}$ signifies a unit vector.

Consider the trajectory shown in Figure 14. Intuitively, IS_x should be greater than IS_y and indeed they were computed to be 0.45 and 0.15, respectively.

The blue rectangle corresponds to the path displayed on the test surface. All users missed this 2 mm wide path and moved the slave slightly inwards ~2 mm, as depicted by the dashed line.

References

1. Cleary K. Medical robotics and the operating room of the future. Proceedings of the IEEE Engineering in Medicine and Biology 27th Annual Conference, Shanghai, China, 1–4 September 2005.
2. Taylor RH. Robotics in orthopedic surgery. In *Computer Assisted Orthopaedic Surgery (CAOS)*, Nolte LP, Ganz R (eds). Hogrefe & Huber: Seattle, 1998; 35–41.
3. Pransky J. ROBODOC – surgical robot success story. *Indust Robot* 1997; **24**(3): 231–233.
4. Reginster JY. The prevalence and burden of arthritis. *Rheumatology* 2002; **41**(1): 3–6.
5. Stulberg SD, Picard F, Saragaglia D. Computer assisted total knee arthroplasty. *Operat Techn Orthop* 2000; **10**: 25–39.
6. Wolf A, DiGioia AM III, Jaramaz B. Computer guided total knee arthroplasty. In *Manual of MIS Techniques in Orthopedics*, Scuderi GR, Tria AJ, Berger RA (eds). Springer-Verlag: Berlin, 2005; 390–407.
7. Wolf A, Shoham M, Shnider M, *et al*. Feasibility study of a mini bone-attached robotic system for spinal operations. *Spine* 2004; **29**(2): 220–228.
8. Pechlivanis I, Kiriyanthan G, Engelhardt M, *et al*. Percutaneous placement of pedicle screws in the lumbar spine using a bone-mounted miniature robotic system. *Spine* 2009; **34**(4): 392–398.
9. Plaskos C, Cinquin P, Lavallée S, *et al*. Praxiteles: a miniature bone-mounted robot for minimal access total knee arthroplasty. *J Med Robotics Comput Assist Surg* 2006; **1**(4): 67–79.
10. Wolf A, Jaramaz B, Lisien B, *et al*. MBARS: mini bone-attached robotic system for joint Arthroplasty. *Int J Med Robotics Comput Assist Surg* 2005; **1**: 101–121.
11. Okamura AM. Methods for haptic feedback in teleoperated robot-assisted surgery. *Int J Indust Robot* 2004; **31**: 499–508.
12. Scott JJ, Gray R. A comparison of tactile, visual, and auditory warnings for rear-end collision prevention in simulated driving. *Human Factors* 2008; **50**(2): 264–275.
13. Lécuyer A, Megard C, Burkhardt JM, *et al*. The effect of haptic, visual and auditory feedback on an insertion task on a two-screen workbench. Immersive Projection Technology (IPT) Symposium, 24–25 March 2002; Orlando, FL, USA.
14. van der Meijden OAJ, Schijven AMP. The value of haptic feedback in conventional and robot-assisted minimal invasive surgery and virtual reality training: a current review. *Surg Endosc* 2009; **23**: 1180–1190.
15. Yokokohji Y, Yoshikawa T. Bilateral control of master–slave manipulators for ideal kinematic coupling – formulation and experiment. *Transactions on Robotics and Automation* 1994; **10**: 605–620.
16. Hogan N. Impedance control: an approach to manipulation: Part I – Theory. *J Dynam Syst Measure Control* 1985; **107**: 1–7.
17. Hokayem PF, Spong MW. Bilateral teleoperation: an historical survey. *Automatica* 2006; **42**: 2035–2057.
18. Kazerooni H, Tsay TI, Hollerbach K. A controller design framework for telerobotic systems. *IEEE Trans Control Syst Tech* 1993; **1**(1): 50–62.
19. Bu Y, Daniel RW, McAree PR. Stability analysis of force reflecting telerobotic systems. Proceedings of IROS, 4–8 November 1996; Osaka, Japan.
20. Fite KB, Shao L, Goldfarb M. Loop shaping for transparency and stability robustness in bilateral telemanipulation. *IEEE Trans Robotics Automat* 2004; **20**(3): 620–624.
21. Niemeyer G, Slotine J-JE. Telemanipulation with time delays. *Int J Robotics Res* 2004; **23**(9): 873–890.
22. Hannaford B, Ryu J-H. Time domain passivity control of haptic interfaces. Proceedings of the IEEE International Conference on Robotics and Automation, 21–26 May 2001; Seoul, Korea.
23. Perreault EJ, Kirsch RF. Crago PE. Multijoint dynamics and postural stability of the human arm. *Exp Brain Res* 2004; **157**(4): 507–517.
24. Burdet E, Tee KP, Mareels I, *et al*. Stability and motor adaptation in human arm movements. *Biol Cybern* 2006; **94**(1): 20–32.
25. Xu Y, Hollerbach JM. Identification of human joint mechanical properties from single trial data. *IEEE Trans Biomed Eng* 1998; **45**(8): 1051–1060.
26. Hashtrudi-Zaad K, Salcudean SE. Analysis of control architectures for teleoperation systems with impedance/admittance master and slave manipulators. *Int J Robotics Res* 2001; **20**(6): 419–445.
27. Baier H, Buss M, Schmidt G. Control mode switching for teledrilling based on a hybrid system model. Proceedings of Advanced Intelligent Mechatronics (AIM '97) Conference, 16–20 June 1997; Tokyo, Japan.
28. Bardorfer A, Munih M. Connecting haptic interface with a robot. 10th Mediterranean Electrotechnical Conference (MELECON), 29–31 May 2000; Cyprus.
29. Riviere CN, Rader SR, Thakor NV. Adaptive canceling of physiological tremor for improved precision in microsurgery. *IEEE Trans Biomed Eng* 1998; **45**(7): 839–846.
30. Krebs HI, Ferraro M, Buerger SP, *et al*. Rehabilitation robotics: pilot trial of a spatial extension for MIT–Manus. *J Neuroeng Rehab* 2004; **1**: 5–19.
31. ATI website, Nano 17 page: http://www.ati-ia.com/products/ft/ft_models.aspx?id=Nano17.
32. Tsai M-D, Hsieh M-S, Tsai C-H. Bone drilling haptic interaction for orthopedic surgical simulator. *Comput Biol Med* 2007; **37**(12): 1709–1718.
33. Sewell C, Blevins NH, Peddamatham S, *et al*. The effect of virtual haptic training on real surgical drilling proficiency. Second Joint

EuroHaptics Conference and Symposium on Haptic Interfaces for Virtual Environment and Teleoperator Systems (WHC'07), 22–24 March 2007; Tsukuba, Japan.
34. Ikei Y, Shiratori M. TextureExplorer: a tactile and force display for virtual textures. Proceedings of the 10th Symposium on Haptic Interfaces for Virtual Environment and Teleoperator Systems, 24–25 March 2002; Orlando, FL, USA.
35. Gardner EP, Martin JH, Jessell TM. The bodily senses. In *Principles of Neural Science*, Kandel ER, Schwartz JH, Jessell TM (eds). McGraw-Hill: New York, 2000; 430–450.
36. Glozman D, Shoham M, Fischer A. A surface-matching technique for robot-assisted registration. *Comput Aided Surg* 2001; **6**(5): 259–269.
37. Tan HZ, Srinivasan MA, Eberman B, *et al*. Human factors for the design of force-reflecting haptic interfaces. *Dynam Syst Control* 1994; **55**: 353–359.
38. Ryu D, Song J-B, Choi J, *et al*. Design of a haptic stability observer in frequency domain for stable haptic interaction. SICE–ICASE International Joint Conference, 18–21 October 2006; Busan, South Korea.

DOI: 10.1002/rcs